Materials Today Chemistry 54 (2026) 103643

Contents lists available at ScienceDirect

Materials Today Chemistry

journal homepage: www.journals.elsevier.com/materials-today-chemistry/

Relationship between microstructure, mechanical, and biological response in biomedical Ti–Nb–Cu alloys

L. Peters, B. Manogar, F. Yang, L. Bolzoni *

The University of Waikato, Hamilton, 3240, New Zealand

ARTICLE INFO

Keywords:
Titanium alloys
Powder metallurgy
Mechanical properties
Antibacterial activity
Biocompatibility

ABSTRACT

Titanium alloys are highly used in biomedical applications, especially structural ones, due to their mechanical properties and biocompatibility. However, they are susceptible to pathogenic bacterial infections, a long-lasting challenge of biomaterials exacerbated by the rise of antibiotic resistant bacteria. To address this, novel Ti–Nb–Cu alloys with intrinsic antibacterial capability were developed and characterised in this study. It is found that changing the amount of Nb and Cu brings about manufacturability and microstructural modifications. Specifically, the amount of porosity increases, the microstructure changes from lamellar to β type, and precipitation of the eutectoid Ti_2Cu intermetallic phase occurs as the contents of Nb and Cu increase. Accordingly, the Ti–Nb–Cu alloys become stronger and less ductile, though they do not fail catastrophically. They always form a protective passivation layer against corrosion, though the corrosion rate is composition dependent. They are characterised by a very strong antibacterial efficacy against both gram negative and gram positive bacteria, and they are not cytotoxic. This combination makes the developed Ti–Nb–Cu alloys promising candidates for structural biomedical applications.

1. Introduction

Materials have been used for biomedical applications from thousands of years; however, biomaterials became much more readily available and used in the 1940's [1]. Metals are the preferred biomaterial choice for medical implants due to their capability of withstanding cyclic loads over long periods of time. They are, therefore, employed to manufacture artificial joints, screws, plates, and prostheses among others, aiming to replace or support failed bones [2,3]. Among metals used in biomedicine, Ti alloys are generally preferred due to three main aspects: high strength to density ratio (i.e. specific properties), low stiffness among structural metallic biomaterials, and biocompatibility [4]. High specific properties means that lighter devices with high mechanical strength can be produced. The low rigidity is beneficial to enhance the transfer of loads from the prosthesis to the human bone, reducing the so-called stress shielding effect [5]. It is worth mentioning that, although Ti alloys have relatively low Young modulus, this is still significantly higher than that of the human bones where this mismatch eventually causes loosening of the implanted prosthesis. Biocompatibility means that the implanted prosthesis is not rejected by the human body's immune system [6].

Metallic biomaterials, as other metallic products, are commonly manufactured using wrought metallurgy, generally consisting of the initial casting of the semi-finished product which is subsequently plastically deformed to impart the desired final shape and properties. Post manufacturing treatments like heat treatments or superficial modifications can also be applied to change the response of the material [7,8]. Powder metallurgy is an alternative manufacturing method to obtain high performance materials, and it is adoption for the manufacturing of metallic biomaterials brings along added advantages like the ability to manufacture porous materials for enhanced bio-integration. The classical powder metallurgy route involves selection of the starting powder (s), blending or mixing, shaping of the loose powders into the desired shape, and conversion of the mechanically interlocked pressed powder particles into chemically bonded particles through sintering [9].

Typical Ti alloys widely used in biomedicine are pure Ti [10,11] and the Ti–6Al–4V alloy [12]; compositions are in mass percentage unless specified differently. Concerns about the cytotoxicity of Al [13,14] and V [15] led to the development of V-free (e.g. Ti–6Al–7Nb [16]) and Al-free (e.g. Ti–13Nb–13Zr [17]) Ti alloys, whilst reduction of the stiffness of the material has been addressed by developing beta Ti alloys (e.g. Ti–35Nb–7Zr–5Ta or TNZT [18]). Significant research is still under

* Corresponding author.
E-mail address: leandro.bolzoni@waikato.ac.nz (L. Bolzoni).

https://doi.org/10.1016/j.mtchem.2026.103643
Received 17 February 2026; Received in revised form 26 March 2026; Accepted 20 April 2026
Available online 27 April 2026
2468-5194/© 2026 The Authors. Published by Elsevier Ltd. This is an open access article under the CC BY license (http://creativecommons.org/licenses/by/4.0/).

way to develop Ti alloys with enhanced mechanical performance, lower manufacturing costs, and added functionality, all of which can be pursued by means of the correct selection of the alloying elements. Specifically, all the elements added to Ti will, to some extent, improve the mechanical behaviour [19,20], but specific alloying elements need to be used to reduce the Young modulus. Reduction of the intrinsic cost is obtained by using alloying elements whose market value is lower than that of Ti. Finally, added functionality such as enhance osteointegration can be achieved using particular elements, which for biomedical applications is primarily restricted to non-toxic elements. Among all the possible alloying elements, Nb is more expensive than Ti, but it is commonly used to reduce the Young modulus, and Cu is cheaper than Ti and has been considered to provide antibacterial capability to Ti alloys. Even though both elements stabilise the β Ti phase, their intrinsic effect is different as Nb is an isomorphous and Cu is a eutectoid alloying element.

The addition of Nb to biomedical Ti alloys has been greatly studied both in binary Ti-xNb alloys (where x = 5-40%) [21–26] and ternary Ti–Nb-X systems, where X was Mn [27], Zr [28], Mo [29], or Ta [30] among others. A range of manufacturing techniques including vacuum arc remelting [21,24,30], cold crucible levitation melting [27,29], press and sinter [26], metal injection moulding without and with hot isostatic pressing [22,23], and spark plasma sintering [25,28] have been explored. In binary Ti-xNb, the addition of Nb changes the equiaxed microstructure of Ti to lamellar α+β for additions lower than 34% and eventually to equiaxed β grains when the Nb content exceeds this value. The brittle ω Ti phase is detected for Nb contents greater than 30% [21]. The stabilisation of a higher amount of β phase and the formation of the ω phase are, respectively, responsible for the initial decrease and subsequent increase of the stiffness. Generally, the strength increases, and the ductility decreases, with the incremental addition of Nb for concentrations up to 34%, point from which the trend is reversed. The addition of Nb also increases the corrosion resistance [23], and does not change the cytotoxicity with respect to pure Ti [24].

The addition of Cu to biomedical Ti alloys has been investigated both in binary Ti-xCu (where x = 2-25%) [31–35] and ternary systems, where the main approach was to add Cu to commercial Ti alloys compositions like Ti–6Al–4V [36] and Ti–5Al-2.5Fe [37]. Either casting [31,33,36] or solid state processes like vacuum hot pressing [32,35,37] and press and sinter [34] were used for their manufacturing. The progressive addition of Cu to Ti leads to the formation of a lamellar α+β microstructure but, conversely to Nb, Cu does not permit to obtain beta Ti alloys. Instead, a eutectoid microstructure composed of α+β Ti phases and Ti_2Cu precipitates is formed for Cu contents >2.0%. The incorporation of Cu in Ti alloys generally leads to an increase in strength, a decrease in ductility, and functionalises the material with antibacterial capability [32,33,35–37] without increasing cell toxicity [35].

The joint effect of the simultaneous addition of Nb and Cu to Ti to create biomedical Ti alloys has been considered by He et al. [38], Takahashi et al. [39], and Li et al. [40]. Specifically, He et al. [38] analysed the fabrication of superelastic Ti–40Nb-(0-10)Cu alloys via spark plasma sintering reporting a high antimicrobial activity due to the presence of Cu. The alloys showed better inhibitory activity against bacteria (*E. coli* and *S. aureus*) than fungi (*C. albicans*). Takahashi et al. [39] reported the mechanical properties of a series of 15 different Ti-(5-30)Nb-(2-20)Cu alloys obtained via ingot casting followed by bench-cooling, concluding that 4 of them can be used for dental prostheses. Finally, Li et al. [40] worked on the development of low-modulus Ti–35Nb-(0-4)Cu alloys aiming at achieving antibacterial behaviour through the addition of Cu. The samples were fabricated via arc-melting, followed by homogenisation at 1000 °C for 12 h, water quenching, and final hot rolling at 1000 °C. The antibacterial rate increased with the amount of Cu. From literature it is, thus, found that very high amounts of Nb are generally targeted and casting was primarily explored for producing Ti–Nb–Cu alloys. To fill gaps, the aim of this work is to explore the design, manufacturing, and characterisation of new ternary Ti–Nb–Cu alloys with relatively low amount of Nb and manufactured by means of powder metallurgy. In particular, the physical properties, mechanical behaviour, and biological response of these new alloys obtained via the press and sinter approach was investigated and quantified. The aim was to identify their interrelationships, and prove their biocompatibility and antibacterial capability. It is worth mentioning that the specific alloying elements where chosen because of their proven biological response. Specifically, Nb is regarded as non-cytotoxic and its addition contributes to the reduction of the stiffness of Ti and enhances the biocompatibility. Conversely, Cu is renown to confer antibacterial properties when added to Ti alloys. Thus, the aim was to strike a balance between biocompatibility and antibacterial properties. As cost was also an issue that was addressed, ternary Ti–Nb–Cu alloys were preferred over more complex alloys which bear additional expensive elements like Zr such as in the Ti–Nb–Zr–Cu alloys [41].

2. Experimental procedure

The raw materials for this study were a hydride-dehydride (HDH) pure Ti powder with irregular morphology (D_{90} < 75 μm, purity >99.4%), a pure Nb powder with angular morphology (D_{90} < 45 μm, purity >99.8%), and a pure Cu powder with dendritic morphology (D_{90} < 63 μm, purity >99.7%). Three ternary Ti–Nb–Cu alloys with Nb to Cu ratio of 1:1 were produced. They are reported in Table 1 along with their density calculated by means of the rule of mixtures. It is worth mentioning that pure Ti and the Ti–2Nb alloy were also considered as reference materials to assess the microstructural changes and the mechanical behaviour. The theoretical density of the Nb-bearing alloys increases with the addition of the alloying elements as both Nb (8.57 g/cm^3) and Cu (8.96 g/cm^3) have higher density than pure Ti (4.50 g/cm^3). The powders were mixed in a V-blender for 30 min using a frequency of 45 Hz to ensure homogenisation of the distribution of the powder particles before their shaping into 40 mm diameter samples through cold uniaxial pressing at 600 MPa. The shaped samples were then sintered under vacuum (10^{-3} Pa) at a maximum temperature of 1300 °C for 2 h using heating and cooling rates of 10 °C/min.

For the characterisation of the microstructure, the alloys were cut, ground with SiC papers, and polished using a colloidal silica suspension. Revealing of the microstructural phases was done by chemical etching by means of a water-based Kroll solution: 4 vol% of HF and 5 vol% of HNO_3. The microstructure was analysed through both optical (Olympus BX60) and electron (Hitachi S4700) microscopy aiming to understand the distribution of the expected residual porosity and Ti phases. XRD (X-ray diffraction) 30-80° patterns of the sintered alloys were obtained by scanning the materials every 0.013° with dwell time of 0.5 s by means of Panalytical X'pert equipment. The dimensions (i.e. diameter and thickness) of the samples, as measured using a 2-decimal calliper, and the weight of the samples, as measured using a 4-decimal balance, were used to calculate the density after pressing. The water displacement method (ASTM B962) was used to quantify the density of the sintered samples. Relative density values, either before or after sintering, were calculated by dividing the density values by the theoretical density of each alloy (Table 1). The densification parameter [42] was used to elucidate the effectiveness of the sintering process, and the effect of the

Table 1
Composition and theoretical density of the alloys considered in this study.

Material	Ti [wt. %]	Nb [wt. %]	Cu [wt. %]	Theoretical density [g/cm^3]
Ti	100	-	-	4.50
Ti–2Nb	98	2	-	4.58
Ti–2Nb–2Cu	96	2	2	4.67
Ti–6Nb–6Cu	88	6	6	5.01
Ti–10Nb–10Cu	80	10	10	5.35

amount of alloying elements used.

For the quantification of the tensile behaviour, 2 × 2 mm^2 dogbone samples with gauge length of 20 mm were cut using electrical discharge machining. A minimum of three samples per composition were cut, and their surface was ground to eliminate its influence. Tensile testing was performed on an Instron 33R4204 using a strain rate of 5×10^{-3} s^{-1}. The elongation of the samples was recorded using an external mechanical extensometer and the offset method was used to calculate the yield stress. Rockwell hardness measurements (minimum of five per sample) were done to quantify the hardness of the ternary Ti–Nb–Cu alloys and the reference alloys.

Electrochemical properties of the samples were determined by using a three-electrode configuration on an electrochemical workstation (eDAQ e-corder 410) at room temperature in HBSS (i.e., Hanks' balanced salt solution). A silver/silver chloride electrode and a platinum electrode served, respectively, as reference and counter electrode meanwhile the samples were the working electrode. A scanning rate of 50 $mV{\cdot}s^{-1}$ from −2 V to 2 V was used to generate the potentiodynamic polarisation curves, from which the corrosion potential E_c and the corrosion current density i_c were then determined. The corrosion rate was estimated as $M{\cdot}i_c/n{\cdot}F$ where M is the molar mass of titanium (g/mol), n is the valency number, and F is the Faraday constant (96,485C/mol).

Antibacterial properties of the sintered alloys were quantified using gram negative *E. coli* (DH5-α) and gram positive *S. aureus* (MRSA 4549) bacteria, which were incubated and cultured in a Luria Broth base overnight for determining their absorbance via a BioRad Smart-specTM 3000 spectrophotometer. Calculation of the CFU, the colony-forming unit, was subsequently performed using 10^{-2}, 10^{-4}, and 10^{-6} serial dilutions. Following the Japanese Industrial Standard JIS 2801:2010 [43], with minor modifications, the *in-vitro* plate count method was used on three replicates placed inside a 12-well culture plate with 30 μl of bacterial culture for their incubation at 37 °C for 1 day. A PBS solution was used to isolate the bacteria, which were then incubated overnight at 37 °C on LB agar-bearing petri dishes. The antibacterial rate was calculated using Eq. (1):

$$Antibacterial\ rate = \left(1 - \frac{CFU_{sample}}{CFU_{control}}\right) x\ 100\ [\%] \qquad \text{Eq. 1}$$

Commercially available *HeLa* cell lines (ATCC) were used to measure the cell viability response. Foetal Bovine Serum and MEM Eagle's solution were used as base media to which different amounts of Penicillin as antibiotic was added. After centrifugation of the cell-bearing media for supernatant removal, the cell growth was promoted via incubation at 37 °C with 5% CO_2. After few passages, Alamar Blue (Invitrogen™, USA) was used as viability assay, measuring the cells concentration at exposure. Pure media (negative control), *HeLa* cells (positive control), and autoclaved specimens were loaded into a 24-well plate using 1×10^6 cells/ml concentration, equivalent to 500 μl of liquid. After 1 day, 3 days, and 5 days of incubation, a mixture of Eagle's solution and Alamar blue (ratio 9:1) was added and incubated at 37 °C for 4 h. The cell viability was determined using a Thermo Scientific Multiskan Go reader.

For both antibacterial and cell viability tests, the results are shown as the arithmetic mean ± one standard deviation. Analysis of the results was carried out using the *t*-test, with statistically significant difference levels of $^{*}p < 0.01$, $^{\#}p < 0.05$ and $^{\dagger}p < 0.1$.

3. Results

Fig. 1 shows the microstructure of the alloys considered in the study. Regardless of the composition, all the materials are characterised by the presence of a uniform distribution of spherical pores primarily located at the grain boundaries; although some few pores are also present the in middle of the grains. In terms of microstructural features, pure Ti is composed of equiaxed α Ti grains (Fig. 1a), and the initial addition of Nb, which is an isomorphous β stabiliser, changes the equiaxed structure to a lamellar structure in the Ti–2Nb alloy (Fig. 1b). The subsequent addition of Cu in the Ti–2Nb–2Cu alloy, where Cu is a eutectoid β stabiliser, does not change the nature of the lamellar structure (Fig. 1c). However, the further increment of the amount of alloying elements progressively refines the lamellar microstructure (Fig. 1d) and, eventually, leads to a β type microstructure in the Ti–10Nb–10Cu alloy (Fig. 1e). XRD analysis (Fig. 1f) shows that the α and β Ti phases are generally present in the Ti–Nb–Cu alloys, the eutectoid Ti_2Cu intermetallic phase is found when the Cu content is greater than 2% (i.e., 6% in this instance), and the α' phase precipitates in the Ti–10Nb–10Cu alloy.

Fig. 2, which shows the SEM micrographs of the Nb-bearing Ti alloys, primarily confirms the results of optical microscopy where the

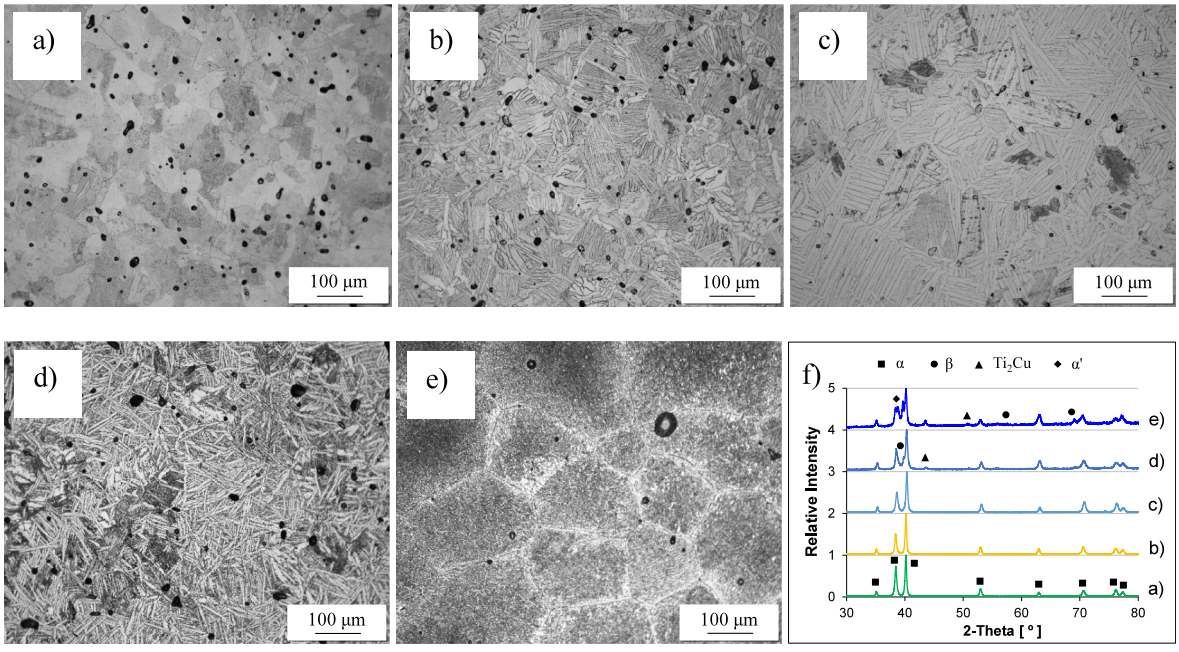

Fig. 1. Optical micrographs of the pressed and sintered Nb-bearing Ti alloys: a) Ti, b) Ti–2Nb, c) Ti–2Nb–2Cu, d) Ti–6Nb–6Cu, e) Ti–10Nb–10Cu, and f) XRD patterns.

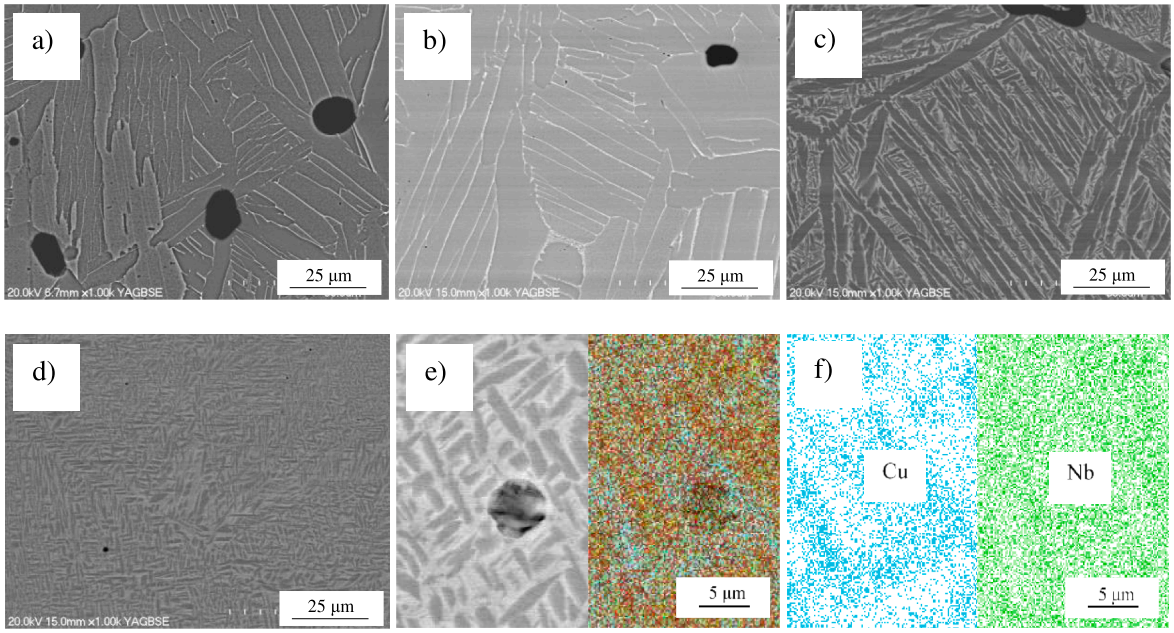

Fig. 2. SEM micrographs of the pressed and sintered Nb-bearing Ti alloys: a) Ti–2Nb, b) Ti–2Nb–2Cu, c) Ti–6Nb–6Cu, and d) Ti–10Nb–10Cu, and representative elemental maps of the distribution of the alloying elements (i.e. Ti–10Nb–10Cu alloy): e) combined maps, and f) Cu and Nb maps.

progressive addition of Cu refines the size of the α+β lamellae, and reduces the interlamellar spacing. From Fig. 2e–f), which shows the elemental mapping distribution of the alloying elements in the Ti–10Nb–10Cu alloy, it can be seen that the composition of the alloy is fully homogenous, though partitioning of the alloying elements between the phases occurs. It is worth mentioning that, as the Ti–10Nb–10Cu alloy has a homogeneous distribution of the alloying elements, the same is found for less heavily alloyed Ti–Nb–Cu alloys where the amount of initial Nb and Cu particle that need to dissolve within the Ti matrix is much lower.

The variation of the density and porosity (both before and after sintering), as well as that of the associated densification, is presented in Fig. 3. The density of the pressed samples is initially fairly constant and, subsequently, increases. This results in a monotonic increment of the amount of porosity found in both the pressed and sintered alloys as a function of the amount of alloying elements added. Moreover, it can be seen that the gap between the porosity of the pressed and sintered samples does also increase with the total amount of alloying elements added, being 8.2% for the Ti–2Nb alloy and 11.1% for the Ti–10Nb–10Cu alloy. In terms of densification, it can be seen that pure Ti, Ti–2Nb and Ti–2Nb–2Cu have a similar value, which subsequently significantly decreases for a higher additions of alloying elements.

Representative stress-strain curves are presented in Fig. 4 where it can be seen that, regardless of the composition, all the sintered materials are characterised by both elastic and plastic deformation behaviour (Fig. 4a). The results of the fractographic analysis performed on the broken tensile samples are in agreement with the tensile data as the fracture surface of pure Ti, Ti–2Nb, Ti–2Nb–2Cu, and Ti–6Nb–6Cu is primarily composed of dimples typical of a fully ductile fracture. However, it can also be noticed that the size of the dimples changes with the type of material, the fracture surface flatness is different, and features related to more brittle transgranular fracture are present when Cu is added as alloying elements. The Ti–10Nb–10Cu alloy has a fairly flat fracture surface with characteristic river patterns.

The variation of the average mechanical properties is presented in Fig. 5 where it can be seen that the addition of the isomorphous β stabiliser Nb leads to a significant increment of the ductility with respect to Ti. However, the strength (both yield stress and ultimate tensile strength) is not significantly affected as, on average, they are slightly more than 10 MPa higher. The initial addition of the eutectoid β stabiliser Cu to the Ti–2Nb alloys significantly increases the strength at the expenses of the ductility, which is reduced to approximately 15%. The subsequent increment of the Nb and Cu contents in the Ti–Nb–Cu alloys leads to the progressive increment of the strength and the reduction of the ability to withstand plastic deformation. Similarly to the strength, the hardness of the sintered materials increases with the addition of Nb or the simultaneously increment of the Nb and Cu contents.

The results of the characterisation of the corrosion behaviour of the Ti–Nb–Cu alloys are shown in Fig. 6 by means of representative potentiodynamic polarisation curves indicating that the alloys have the

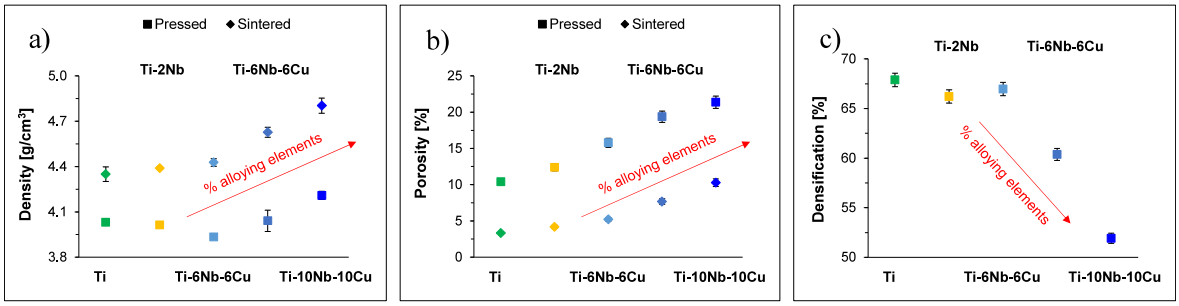

Fig. 3. Physical properties of the pressed and sintered Nb-bearing Ti alloys: a) density, b) amount of porosity, and c) densification.

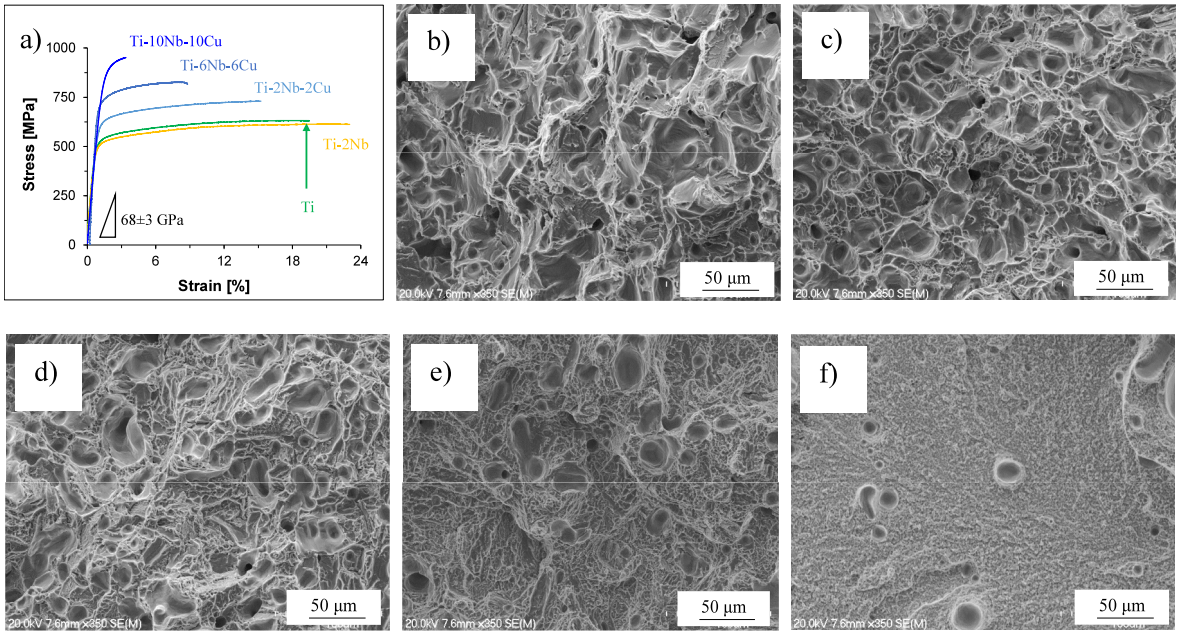

Fig. 4. Representative stress-strain curves (a), and results of the fractographic analysis: b) Ti, c) Ti–2Nb, d) Ti–2Nb–2Cu, e) Ti–6Nb–6Cu, and f) Ti–10Nb–10Cu.

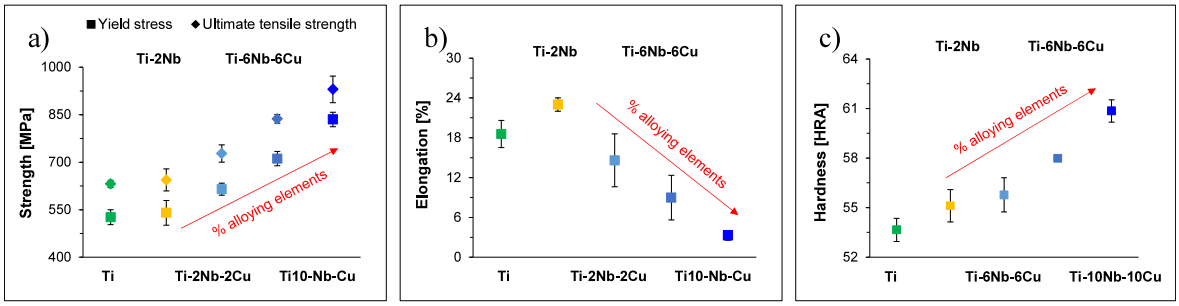

Fig. 5. Mechanical properties of the pressed and sintered Nb-bearing Ti alloys: a) tensile strength (yield stress and ultimate tensile strength), b) elongation, and c) hardness.

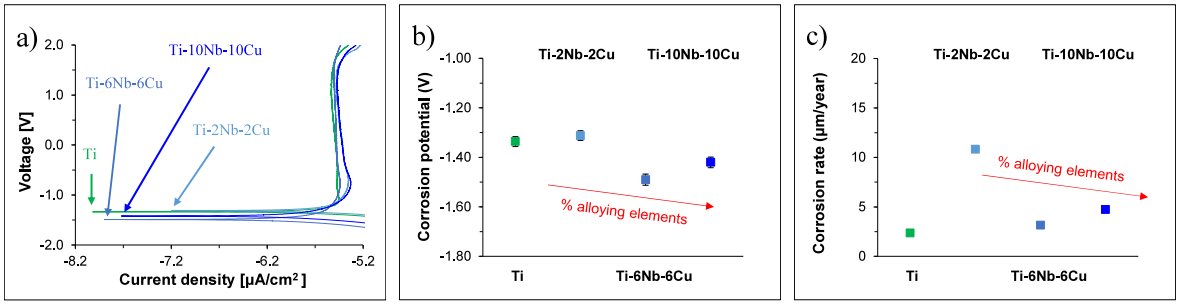

Fig. 6. Corrosion behaviour of the pressed and sintered Nb-bearing Ti alloys: a) potentiodynamic polarisation curves, b) corrosion potential, and c) corrosion rate.

characteristic passivation response of Ti alloys. The actual composition affects both the current density and corrosion potential where the latter, generally, decreases as the amounts of Nb and Cu increase. However, the Ti–6Nb–6Cu alloy has the lowest value. Therefore, the Ti–Nb–Cu alloys have a higher corrosion rate with respect to pure Ti, where the Ti–2Nb–2Cu alloy has the highest corrosion rate of 10.8 µm/year.

Fig. 7 shows the results of the biological response, both antibacterial and cell viability, of the pressed and sintered Nb-bearing Ti alloys. Regardless of their chemistry, the Ti–Nb–Cu alloys have a suitable antibacterial response, which is commonly greater than the minimum 90% threshold reported by the GB4789.2-2016 standard to be considered antibacterial materials. A less straightforward behaviour is obtained in terms of cell viability with a significant impact from the actual exposure time, where the cell viability is affected after 1 day but recovered for longer exposure times. It can also be seen that few of the antibacterial and cell viability behaviours are statistically significant, with all the average data points being Grade 2 (day 1) or above (day 3 and day 5). This indicates that they are not cytotoxic as per the ISO 10993-5/2009 standard grading system.

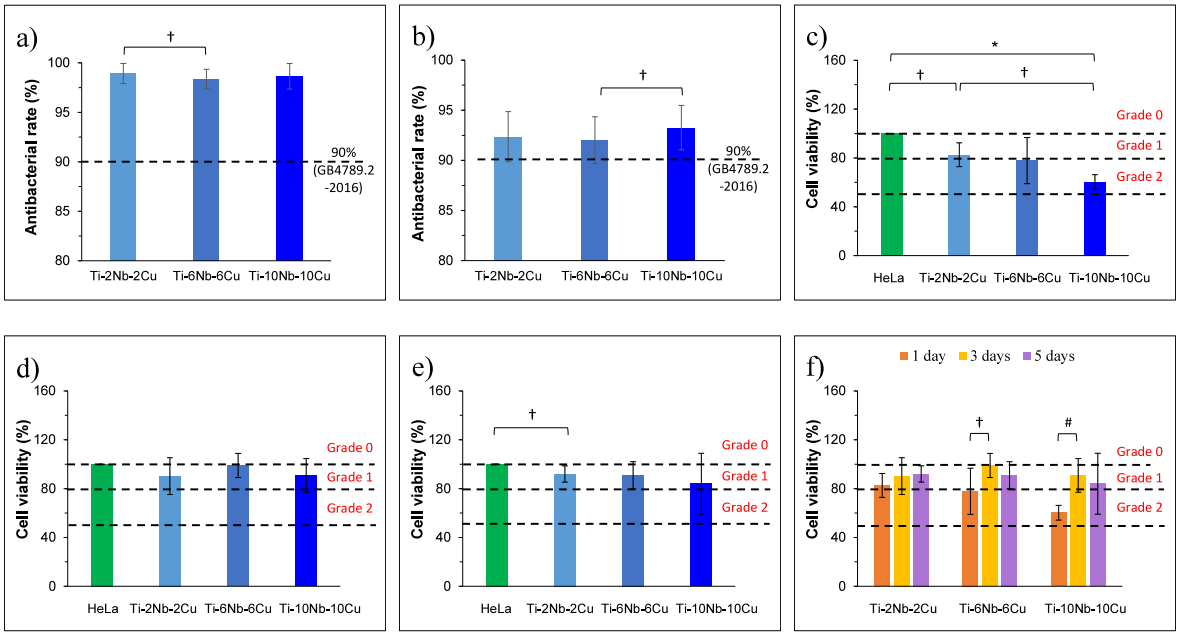

Fig. 7. Biological response of the pressed and sintered Nb-bearing Ti alloys: a) antibacterial rate against *E. coli*, b) antibacterial rate against *S. aureus*, c) cell (*HeLa*) viability at one day, d) cell (*HeLa*) viability at three days, e) cell (*HeLa*) viability at five days, and f) evolution of the cell (*HeLa*) viability with exposure time. *$p < 0.01$, $^{\#}p < 0.05$ and $^{\dagger}p < 0.1$.

4. Discussion

In this study the manufacturing and characterisation of new ternary Ti-(2-10)Nb-(2-10)Cu alloys was considered. Specifically, the alloys were manufactured by means of the blended elemental powder metallurgy approach whilst casting is commonly used in literature. Moreover, relatively lower amounts of Nb were considered compared to literature, where much higher amounts (i.e., 35-40%) [38,40] are the norm. Where possible and sensible, the properties were compared to those of pure Ti and the Ti–2Nb alloy manufactured using the same technique. Microstructural analysis (Fig. 1) shows that the sintered alloys have a uniform distribution of spherical pores primarily located at the grain boundaries in their microstructure. The mean size of the pores seems to be slightly bigger as the amount of alloying elements added to the Ti matrix increases. However, the presence of spherical pores indicates that, under the sintering conditions used in the current study, the alloys reached the last stage of sintering where pore coalescence occurs. Considering the phases present in the microstructure, it is found that pure Ti is composed of equiaxed α Ti grains, whose grain size is comparable to that of the starting HDH powder. This means that no significant grain growth occurred in the material. The addition of Nb changes the equiaxed grains to a lamellar structure in the Ti–2Nb alloy; the lamellar microstructure is typical of α+β Ti alloys slow cooled from above their allotropic phase transformation temperature. In particular, the size of the prior β grains is comparable to that of pure Ti and alternating parallel α+β lamellae are found within each prior β grain. The Ti–2Nb–2Cu alloy still has a lamellar structure, but the incorporation of Cu significantly increases the size of the prior β grains and the width of the α+β lamellae. Further combined additions of Nb and Cu reduce the size of the prior β grains, which is comparable to that of the Ti–2Nb alloy, reduce the width of the α+β lamellae, which are finer that those found in the Ti–2Nb alloy, and reduce the interlamellar spacing. Both the Ti–2Nb–2Cu and Ti–6Nb–6Cu are α+β Ti alloys. The subsequent increment of the Nb and Cu contents to 10% creates a metastable β Ti alloy whose microstructure is composed of equiaxed β grains. The average size of these grains is slightly bigger than the original HDH powder particles, and very fine α′α needle-shaped grains typical of metastable β Ti alloys are also present.

The XRD patterns of the sintered materials (Fig. 1f) show that the reference pure Ti is exclusively composed of peaks related to the hcp crystalline structure of the α Ti phase. Although of the stabilisation of the β Ti phase found during the microstructural analysis of the Ti–2Nb and Ti–2Nb–2Cu alloys, no peaks related to the bcc crystalline structure of the β Ti phase were detected on the XRD patterns of those alloys. This is due to the limitation of the equipment used [44]. However, it can be seen that peaks related to the family planes of the bcc crystalline structure are detected in the XRD patterns of the Ti–6Nb–6Cu and Ti–10Nb–10Cu alloys. Moreover, it can be seen that in these alloys the presence of the eutectoid Ti_2Cu intermetallic phase is also detected. This phase could not be properly identified during the microstructural analysis, but it is expected on the basis of the binary Ti–Cu phase diagrams [45]. Literature reports on the fabrication of binary Ti–Cu alloys show that the eutectoid Ti_2Cu intermetallic phase was found for Cu additions greater than 2% [31–36,39]. Finally, in the Ti–10Nb–10Cu alloys the main peak of the α' phase peak, which was found as needle-like precipitates within the equiaxed β grains (Fig. 1e), was also detected overlapping with the α (002) peak. XRD analysis also hints to the fact that no undissolved alloying elements are present, and this was confirmed by means of SEM-EDS analysis (Fig. 2). In particular, the representative elemental maps of the Ti–10Nb–10Cu alloy, which is the one bearing the greatest among of both Nb and Cu, show a fully homogenous chemistry with no undissolved powder particles of the original alloying elements. More in detail, Nb is homogeneously distributed in both the α and β Ti phases whilst Cu is predominantly found in the β Ti phase. This is in agreement with the, respective, binary Ti–Nb and Ti–Cu phase diagrams [45] as Nb is soluble in the α Ti phase (approx. 4%) whereas the solubility of Cu in the α Ti phase is negligible.

From the analysis of the variation of the physical properties (Fig. 3), it is found that the addition of the Nb and Cu powders initially decreases the density of the pressed samples, which afterwards increases. Similarly, the density of the sintered alloys systematically increases with the total amount of alloying elements added. As the theoretical density of the Ti–Nb–Cu alloys increases with the addition of Nb and Cu, both being heavier that Ti, this means that the differences in terms of particle size distribution, particle morphology, and hardness of the blended raw materials diminish the compressibility of the alloy. In particular, both the initial addition of 2% of Nb to Ti as well as the addition of 2% Cu to

the Ti–2Nb alloy lead to an approximate decreases of 2% of the relative density of the pressed samples. The subsequent addition of more Nb and Cu also leads to a further 2% decrease of the relative density of the pressed samples. As the latter is strongly related to the relative density of the sintered density, the relative density of the sintered specimens has also a decreasing trend with the progressive addition of more alloying elements. Coherently, Fig. 3b) shows that the amount of residual porosity found in the Nb-bearing Ti alloys monotonically increases with the amount of alloying elements. This means that the higher the amount of alloying elements that needs to dissolve within the Ti matrix the lower the relative density of the sintered samples. This behaviour is due to the progressive increase of the Nb content rather than the Cu content. Specifically, Nb has much higher melting point than Ti, and so of Cu, and thus slower diffusivity at a constant temperature, whereas Cu has lower melting point than Ti. From literature, the progressive addition of dendritic Cu particles to a HDH Ti powder in binary Ti–Cu alloys decreases the relative density of the pressed samples, but actually increases the relative density of the sintered samples as the high diffusivity of Cu enhances the densification of the alloy [34]. As a consequence of the concurrent effects that the added powder particles of the alloying elements have on the density of both the pressed and sintered alloys, it is found that the densification level is comparable (~67%) amongst pure Ti and the Ti–2Nb and Ti–2Nb–2Cu alloys. However, lower densification values are then achieved for higher additions of alloying elements. This is because a greater amount of thermal energy needs to be invested for the dissolution and homogenisation of the alloying elements within the microstructure.

The mechanical characterisation of the pressed and sintered Nb-bearing Ti alloys by means of tensile testing shows, through the representative stress-strain curves, that the alloys are able to withstand some plastic deformation after yielding (Fig. 4). The alloys become stronger, and automatically less ductile, as the amount of alloying elements is increased. Hence, the morphology of the dimples present in the fracture surface changes, and the surface itself becomes more flat transitioning to a more brittle behaviour, rather than purely ductile. Specifically, the fracture surface of pure Ti is fairly rough, typical of ductile metals with a hcp lattice and equiaxed microstructure. Subsequently, the fracture surface becomes less rough, practically flat, for the Ti–10Nb–10Cu alloy, which is characterised by complete transgranular fracture. As a general trend, the addition of a progressively higher amount of alloying elements increases the yield stress, the ultimate tensile strength, and the hardness, and decreases the achievable strain. The only exception is the Ti–2Nb alloy, which is slightly stronger than pure Ti but also more ductile (Fig. 5). In this specific case, the increment of the ductility is due to the initial stabilisation of the β phase. In particular, the addition of Nb transforms the microstructure from being composed by equiaxed grains in pure Ti (Fig. 1a) to a lamellar structure (Fig. 1b). More generally, the variation of the mechanical properties and the fracture surface (Fig. 4) is obviously related to the different effects that the addition of the alloying elements have on the manufacturability, microstructure, and phases of the materials. As previously discussed, the addition of Nb and Cu to Ti decrease the achieved relative density, transforms the equiaxed microstructure into lamellar with different features depending on the type and total amount of alloying elements, and the eutectoid Ti_2Cu intermetallic phase is present in the Ti–6Nb–6Cu and Ti–10Nb–10Cu alloys. In order to better understand the specific contribution of the microstructural features, the average mechanical properties are plotted against the amount of porosity present in the sintered samples in Fig. 8. It would generally be expected that the strength and hardness linearly decrease with the increment of the amount of porosity. However, Fig. 8a) shows that both the strength and the hardness of the Nb-bearing Ti alloys linearly increase with the amount of porosity. To prevent misunderstanding, it is worth mentioning that though the trend reported in Fig. 8a) is against the porosity, the trend is actually due to the concurrent effects brought about by the addition of the alloys rather than a causative relationship. In particular, the negative effect induced by the increment of the amount of porosity is overcompensated by the beneficial effects derived by the addition of the alloying elements. These include the formation of a progressively refined lamellar structure, a greater amount of stabilised β Ti phase, and a greater contribution to solution hardening by the alloying elements. Moreover, the precipitation of the eutectoid Ti_2Cu intermetallic phase, notably intrinsically hard and brittle, in the Ti–6Nb–6Cu and Ti–10Nb–10Cu alloys further contributes to increasing the mechanical properties. All of these microstructure-related features hinder the movement of dislocations and contribute to the strengthening of the material. In particular, solution hardening is achieved thanks to the presence of a higher amount of alloying elements dissolved in the lattice, strain hardening is obtained through the formation and refinement of the lamellar structure, and precipitation hardening derives from the eutectoid Ti_2Cu particles. However, it is interesting to note that the hardness of the Nb-bearing Ti alloys increases at a greater rate than its strength, where the yield and ultimate tensile strength have comparable incremental rate. With respect to the ductility of the alloys (Fig. 8b), all the previously mentioned strengthening mechanisms contribute to the embrittlement of the material on top of the presence of a greater number of pores, whose size also increases with the addition of a greater amount of alloying elements.

The potentiodynamic polarisation curves showing the corrosion behaviour of the Ti–Nb–Cu alloys indicate that they are able to form a protective passivation layer regardless of the actual chemistry of the alloy. This means that the concurrent addition of Nb and Cu does not disrupt the ability to self-passivate, though the specific amount of alloying elements added directly changes the corrosion response. With respect to pure Ti, the Ti–2Nb–2Cu alloy has a more positive corrosion potential, and the Ti–6Nb–6Cu and Ti–10Nb–10Cu alloys have a more negative value. This is commonly associated with a lower propensity to release metallic ions. Thus, the Ti–2Nb–2Cu alloy has the highest corrosion rate amongst the alloys studied; however, as the corrosion rate depends also on the current density, it can be seen that the other Ti–Nb–Cu alloys have a slightly higher corrosion rate with respect to pure Ti. This is due to the presence of the alloying elements dissolved onto the Ti lattice. From the potentiodynamic polarisation curves it can also be seen that the slope of the cathodic part of the curve is fairly

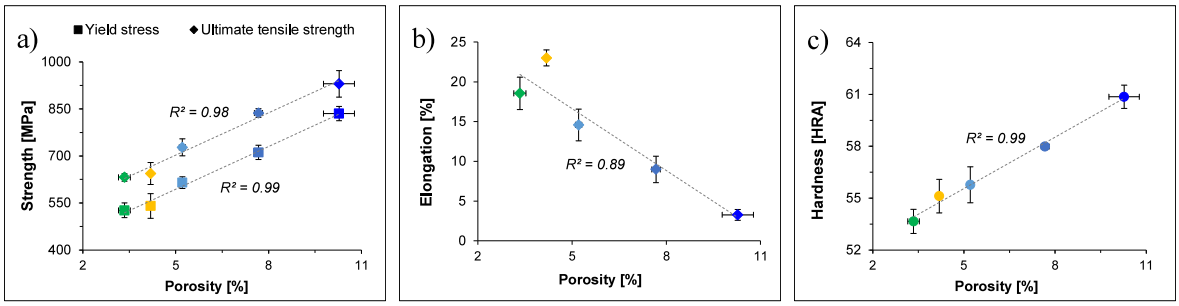

Fig. 8. Mechanical properties of the pressed and sintered Nb-bearing Ti alloys plotted against the porosity level: a) strength, b) elongation, and c) hardness.

constant (i.e., −0.27 ± 0.05 mV/dec) since it related to the Hanks solution corrosion medium. Conversely, the slope of the anodic part of the curve is directly affected by the chemical composition, with values ranging from −11.7 mV/dec for the Ti–2Nb–2Cu alloy to −38.1 mV/dec for the Ti–6Nb–6Cu alloy, clearly showing the effect of the actual resultant microstructure. These data point to the fact that the process is electron-transfer controlled. The actual corrosion response and corrosion rate are, therefore, the compromise between the amount of porosity, which leads to localised changes of the corrosion environment (e.g., oxygen depletion [46]), and the phases present. The latter lead to the formation of local galvanic couples as a function of the partitioning of the alloying elements in the different phases. In particular, it seems that, in this instance, having a refined lamellar microstructure and the precipitation of the eutectoid Ti_2Cu intermetallic phase is beneficial to reduce the corrosion rate of the Ti–Nb–Cu alloys.

The analysis of the antibacterial response of the pressed and sintered Nb-bearing Ti alloys shows that they are effective against both gram negative *E. coli* and gram positive *S. aureus*, with antibacterial rates always greater than 90% (Fig. 7). The average antibacterial rate is slightly higher against *E. coli* (i.e., 98.6 ± 0.3) than *S. aureus* (i.e., 92.5 ± 0.6) where the antibacterial response is attributed to the use of Cu as alloying element, which is known to be one of the most effective natural antibacterial elements [47]. In terms of cell viability as assessed in comparison to *HeLA* cells, it can be seen that the lowest values are obtained after 1 day of exposure, and the viability decreases with the amount of alloying elements added. This hints to the fact that the cells undergo some sort of stress when first exposed to the new environment (i.e., the surface of the Ti–Nb–Cu alloys) and need time to adapt to it. It can then be seen that, despite local variations as a function of the type of alloy and exposure time, there is a general recovery of the cell viability with minimum values of 90.2% after 3 days of exposure and 84.1% after 5 days. The increments from day 1 to day 3 are, generally, statistically significant. Regardless of the actual values, the Ti–Nb–Cu alloys are always considered not cytotoxic on the basis of the guidelines provided by ISO 10993-5/2009 standard.

In order to clarify which of the microstructural features do affect the most the mechanical properties, the corrosion behaviour, and the biological response, as well as to identify hidden relationships, a linear regression heat map was developed and it is presented in Fig. 9. From this analysis, it can be seen that there are very strong correlations amongst the different aspects of the microstructure considered, which include the relative density, the densification, and the inferred amount of stabilised β Ti phase and precipitated eutectoid Ti_2Cu intermetallic phase. This is coherent with the results of the microstructural analysis (Figs. 1 and 2) and of the physical properties (Fig. 3) of the Ti–Nb–Cu alloys. The progressive addition of a greater amount of alloying elements simultaneously changes the resultant amount of porosity and phases present. Not surprisingly, strong interrelations are also found amongst the measured mechanical properties and the microstructural features. For instance, in metals, strength and hardness commonly share a similar trend, which is the opposite to that of ductility, as all of them are controlled by the active strengthening mechanisms and how much dislocations movement is hindered. In this occurrence, the increment of the Nb and Cu contents lead to solid solution strengthening, grain refinement [48], stabilisation of a greater amount of β phase, precipitation of the eutectoid Ti_2Cu intermetallic phase, and higher amount of porosity. All of these factors are detrimental to ductility and all of them, except porosity, are beneficial to enhance plastic deformation resistance

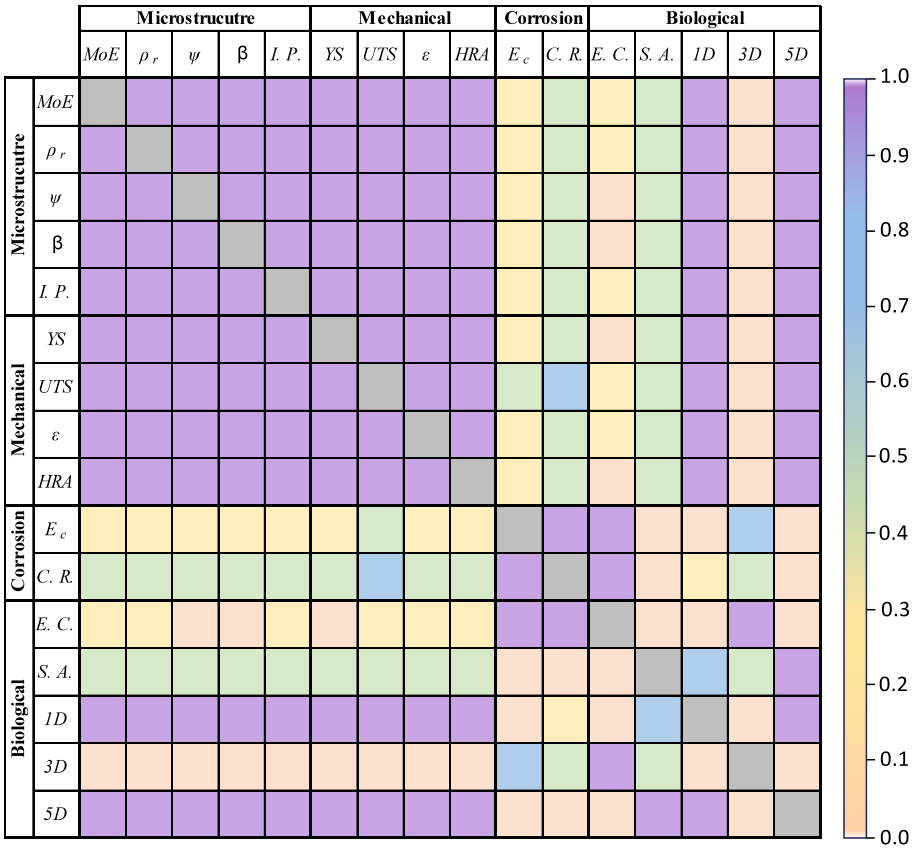

Fig. 9. Linear regression heat map of the interrelationship between microstructural, mechanical, corrosion, and biological response of the pressed and sintered Nb-bearing Ti alloys. Legend: *MoE* – molybdenum equivalent, ρ_r – relative density, ψ – densification, β – relative intensity of the main peak of the β Ti phase in the XRD pattern, *I. P.* – relative intensity of the main peak of the Ti_2Cu intermetallic phase in the XRD patter, *YS* – yield stress, *UTS* – ultimate tensile strength, ε – elongation, *HRA* – hardness, E_c – corrosion potential, *C. R.* – corrosion rate, *E. C.* – antibacterial rate against *E. coli*, *S. A.* – antibacterial rate against *S. aureus*, *1D* – cell viability at 1 day, *3D* – cell viability at 3 days, and *5D* – cell viability at 5 days.

(Fig. 5). Microstructural features, and accordingly mechanical properties in this occasion, have a significantly lower correlation with the corrosion behaviour and the biological response as both are affected by the formation of a passivation layer (Fig. 6) and localised phenomena happening on the surface of the Ti–Nb–Cu alloys. However, it is found that the microstructural features strongly affect the cell viability at 1 and 5 days of exposure, as *HeLa* cells are initially stressed by coming into contact with Ti–Nb–Cu alloys and then they recover. There is strong correlation between corrosion potential and corrosion rate, and they both have an impact on the response of the *E. coli* bacteria, but not on other bacteria/cells. This is most likely due to the characteristic less pronounced peptidoglycan wall and presence of both an outer and a cytoplasmic membrane of gram negative bacteria [47]. The specific response of the bacteria and cell strains used (i.e., DH5-α for *E. coli*, MRSA 4549 for *S. aureus*, and ATCC for *HeLa* cells) also leads to some unusual correlations between particular aspects of the quantified overall biological response.

Fig. 10 shows a comparison of the mechanical behaviour of the pressed and sintered Nb-bearing Ti alloys of this study with binary Ti–Nb alloys [21,22], binary Ti–Cu alloys [31,34,49], Ti–Cu–Mn [50–54], Ti–Nb–Cu alloys [39,40], Ti–Nb–Zr–Cu alloys [41], and common biomedical Ti-based alloys [55]. From Fig. 10a), it can be seen that the sintered Nb-bearing Ti alloys of this study have better yield stress/elongation balance than most materials including sintered binary Ti–Nb alloys, cast binary Ti–Cu alloys, sintered binary Ti–Cu alloys, sintered Ti–Cu–Mn alloys, and other Ti–Nb–Cu alloys. The performance are comparable to those of cast binary Ti–Nb alloys with high Nb content (14-26%) and slightly lower, at least in term of yield stress for the same elongation, with respect to wrought Ti alloys commonly used in biomedicine (e.g., Ti–6Al–4V). The Ti–Nb–Zr–Cu alloys are generally stronger and more ductile as obtained via casting plus heat treatment. The differences in terms of mechanical performance are obviously related to the differences in terms of microstructural features (i.e. presence of porosity, phases, and characteristics of the lamellar structure) and the oxygen content, which is generally expected to be higher in sintered Ti alloys produced from HDH powder [12,16,22,56,57], with respect to wrought Ti alloys. Similar behaviour is found for the ultimate tensile strength/hardness balance where the Nb-bearing Ti alloys of this study generally have better or comparable ultimate tensile strength, but lower hardness compared to other Ti alloys either wrought, cast, or sintered.

A comparison of the antibacterial response of the pressed and sintered Nb-bearing Ti alloys of this study with literature [32,38,40,50–54,58–61] is presented in Fig. 11 for both gram negative and gram positive bacteria. From the comparison, it can be seen that the alloys developed in this study are amongst the most effective antibacterial Cu-bearing alloys, regardless of their composition and the type of bacteria considered. Some of the binary Ti-xCu and ternary Ti–Nb–Cu alloys stand out as having an antibacterial rate lower than minimum threshold of 90%, despite bearing Cu as alloying element. This is mainly due to the combination of actual amount of Cu used as alloying element and the manufacturing parameters used, which change the resultant microstructural features. In literature, the presence of Ti_2Cu has been reported to enhance the antibacterial response of Cu-bearing Ti alloys [32,33,35–37].

5. Conclusions

This study investigated the development of novel Ti–Nb–Cu alloys manufactured by means of the blended elemental powder metallurgy approach and characterised their microstructure, physical properties, mechanical performance, corrosion behaviour, and biological response. The addition of a progressively greater amount of Nb and Cu to Ti affects both the manufacturability (e.g., densification) and the resultant structure. The Ti–Nb–Cu alloys are characterised by a homogenous distribution of residual pores, whose total amount increases with the alloying elements content, and a lamellar microstructure that becomes finer and transition to a β type microstructure for a sufficiently high amount of alloying elements, 10 wt percentage in this instance. The increase of the Cu content also eventually leads to the precipitation of the eutectoid Ti_2Cu intermetallic phase. Homogenisation of the chemistry of the alloy is always achieved with the manufacturing parameters used, regardless of the actual chemical composition of the Ti–Nb–Cu alloys. As a consequence of the described microstructural changes, the Ti–Nb–Cu alloys become progressively stronger and harder, but less ductile, as the amount of alloying elements is increased due to the several strengthening mechanisms which are activated (e.g., microstructural refinement, and precipitation). Nevertheless, the Ti–Nb–Cu alloys always undergo plastic deformation upon tensile loading, indicating a non-catastrophic failure, though the fracture mode transition from pure ductile to transgranular. Very strong correlations are found between and amongst the several microstructural and mechanical properties analysed. Irrespective of their chemistry, the Ti–Nb–Cu alloys show the characteristic passivation response of Ti alloys, meaning that the concurrent addition of Nb and Cu does not interfere with its formation. However, the overall corrosion behaviour, and so the corrosion rate, are composition dependent, with the process being controlled by transfer of electrons. In terms of biological response, the Ti–Nb–Cu alloys developed in this study are very effective against both gram negative and gram positive bacteria as tested against *E. coli* and *S. aureus*, where the effectiveness is slightly better in the former case. The pressed and sintered Ti–Nb–Cu alloys are also not cytotoxic, even though the cell viability results clearly indicate that cells need time to adapt to the exposure to the alloys and, especially in the early stages, there is a clear effect from their chemistry as it determines the microstructural features that comes into contact with the cells.

CRediT authorship contribution statement

L. Peters: Methodology, Investigation. **B. Manogar:** Methodology, Investigation, Formal analysis. **F. Yang:** Methodology, Investigation. **L. Bolzoni:** Writing – review & editing, Methodology, Investigation,

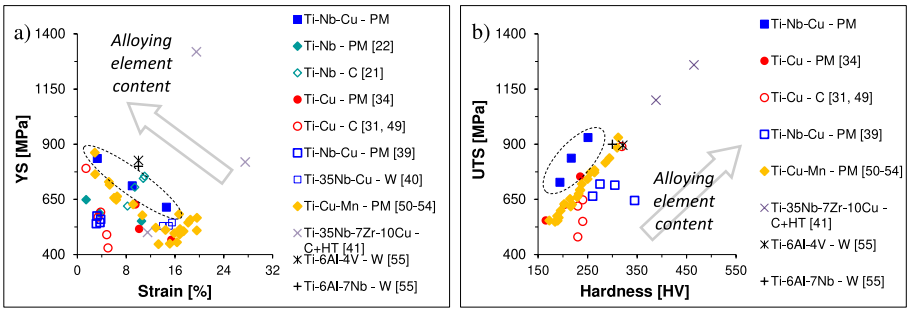

Fig. 10. Comparison of the mechanical properties of the pressed and sintered Nb-bearing Ti alloys with literature: a) yield stress vs elongation, and b) ultimate tensile strength vs hardness. Legend: *PM* – powder metallurgy, *C* – casting, *HT* – heat treatment, and *W* – wrought.

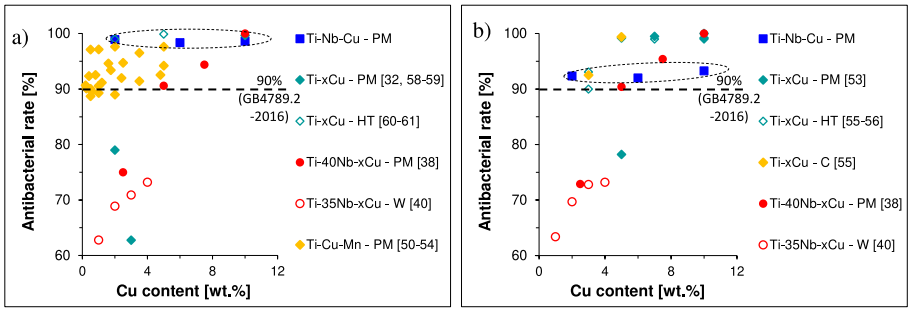

Fig. 11. Comparison of the antibacterial response of the pressed and sintered Nb-bearing Ti alloys with literature: a) antibacterial rate vs. Cu content for gram negative bacteria (i.e., *E. coli*), and b) antibacterial rate vs. Cu content for gram positive bacteria (i.e., *S. aureus*). Legend: *PM* – powder metallurgy, *C* – casting, and *W* – wrought.

Formal analysis, Conceptualization.

Declaration of competing interest

The authors declare that they have no known competing financial interests or personal relationships that could have appeared to influence the work reported in this paper.

Acknowledgements

This research did not receive any specific grant from funding agencies in the public, commercial, or non-profit sectors. The authors would also like to thank Mr. M. Alqattan for his technical contribution.

Data availability

Data will be made available on request.

References

[1] M.F.F.A. Hamidi, W.S.W. Harun, M. Samykano, S.A.C. Ghani, Z. Ghazalli, F. Ahmad, A.B. Sulong, A review of biocompatible metal injection moulding process parameters for biomedical applications, Mater. Sci. Eng. C 78 (2017) 1263–1276.
[2] M. Niinomi, Mechanical biocompatibilities of titanium alloys for biomedical applications, J. Mech. Behav. Biomed. Mater. 1 (1) (2008) 30–42.
[3] M.T. Jia, B. Gabbitas, L. Bolzoni, Evaluation of reactive induction sintering as a manufacturing route for blended elemental Ti-5Al-2.5Fe alloy, J. Mater. Process. Technol. 255 (2018) 611–620.
[4] M. Niinomi, Mechanical properties of biomedical titanium alloys, Mater. Sci. Eng. 243 (1–2) (1998) 231–236.
[5] M. Long, H.J. Rack, Titanium alloys in total joint replacement - a materials science perspective, Biomaterials 19 (18) (1998) 1621–1639.
[6] M. Geetha, A.K. Singh, R. Asokamani, A.K. Gogia, Ti based biomaterials, the ultimate choice for orthopaedic implants - a review, Prog. Mater. Sci. 54 (3) (2009) 397–425.
[7] X. Liu, P.K. Chu, C. Ding, Surface modification of titanium, titanium alloys and related materials for biomedical applications, Mater. Sci. Eng. R Rep. 47 (3–4) (2004) 49–121.
[8] S. Wang, Z. Liao, Y. Liu, W. Liu, Influence of thermal oxidation duration on the microstructure and fretting wear behavior of Ti6Al4V alloy, Mater. Chem. Phys. 159 (2015) 139–151.
[9] L. Bolzoni, P.G. Esteban, E.M. Ruiz-Navas, E. Gordo, Mechanical behaviour of pressed and sintered titanium alloys obtained from master alloy addition powders, J. Mech. Behav. Biomed. Mater. 15 (2012) 33–45.
[10] M. Niinomi, Recent metallic materials for biomedical applications, Metall. Mater. Trans. 33 (3) (2002) 477–486.
[11] S. Raynova, Y. Collas, F. Yang, L. Bolzoni, Advancement in the pressureless sintering of CP titanium using high-frequency induction heating, Metall. Mater. Trans. 50 (10) (2019) 4732–4742.
[12] P. Kumar, K.S.R. Chandran, Strength-ductility property maps of powder metallurgy (PM) Ti-6Al-4V alloy: a critical review of processing-structure-property relationships, Metall. Mater. Trans. 48 (5) (2017) 2301–2319.
[13] D.P. Perl, Relationship of aluminum to alzheimer's disease, Environ. Health Perspect. (1985) 149–153.
[14] K. Klotz, W. Weistenhöfer, F. Neff, A. Hartwig, C. van Thriel, H. Drexler, The health effects of aluminum exposure, Deutsches Arzteblatt international 114 (2017) 653–659.
[15] J.L. Domingo, Vanadium and tungsten derivatives as antidiabetic agents: a review of their toxic effects, Biol. Trace Elem. Res. 88 (2002) 97–112.
[16] Y. Itoh, H. Miura, T. Uematsu, K. Sato, M. Niinomi, Improvement of the properties of Ti-6Al-7Nb alloy by metal injection molding, advances in powder metallurgy & particulate materials proceedings of the 2007 international conference on powder metallurgy & particulate materials, May 13–16, Denver, Colorado (Part 4—Powder Injection Molding (Metals & Ceramics)) 4 (2007) 81–86.
[17] V.A.R. Henriques, E.T. Galvani, S.L.G. Petroni, M.S.M. Paula, T.G. Lemos, Production of Ti-13Nb-13Zr alloy for surgical implants by powder metallurgy, J. Mater. Sci. 45 (21) (2010) 5844–5850.
[18] L.M. Zou, C. Yang, Y. Long, Z.Y. Xiao, Y.Y. Li, Fabrication of biomedical Ti-35Nb-7Zr-5Ta alloys by mechanical alloying and spark plasma sintering, Powder Metall. 55 (1) (2012) 65–70.
[19] L. Bolzoni, P.G. Esteban, E.M. Ruiz-Navas, E. Gordo, Influence of powder characteristics on sintering behaviour and properties of PM Ti alloys produced from prealloyed powder and master alloy, Powder Metall. 54 (4) (2011) 543–550.
[20] L. Bolzoni, E.M. Ruiz-Navas, E. Gordo, Influence of vacuum hot-pressing temperature on the microstructure and mechanical properties of Ti-3Al-2.5V alloy obtained by blended elemental and master alloy addition powders, Mater. Chem. Phys. 137 (2012) 608–616.
[21] Y.-H. Hon, J.-Y. Wang, Y.-N. Pan, Composition/phase structure and properties of titanium-niobium alloys, Mater. Trans. 44 (11) (2003) 2384–2390.
[22] D. Zhao, K. Chang, T. Ebel, M. Qian, R. Willumeit, M. Yan, F. Pyczak, Microstructure and mechanical behavior of metal injection molded Ti-Nb binary alloys as biomedical material, J. Mech. Behav. Biomed. Mater. 28 (2013) 171–182.
[23] E. Yılmaz, A. Gökçe, F. Findik, H.O. Gulsoy, Metallurgical properties and biomimetic HA deposition performance of Ti-Nb PIM alloys, J. Alloys Compd. 746 (2018) 301–313.
[24] Y. Zhang, D. Sun, J. Cheng, J.K.H. Tsoi, J. Chen, Mechanical and biological properties of Ti-(0-25 wt%)Nb alloys for biomedical implants application, Regen. Biomater. 7 (1) (2020) 119–127.
[25] D. Kalita, Ł. Rogal, T. Czeppe, A. Wójcik, A. Kolano-Burian, P. Zackiewicz, B. Kania, J. Dutkiewicz, Microstructure and mechanical properties of Ti-Nb alloys prepared by mechanical alloying and spark plasma sintering, J. Mater. Eng. Perform. 29 (3) (2020) 1445–1452.
[26] D.R. Santos, V.A.R. Henriques, C.A.A. Cairo, M.S. Pereira, Production of a low young Modulus titanium alloy by powder metallurgy, Mater. Res. 8 (2005) 439–442.
[27] Z. Chen, Y. Liu, H. Jiang, M. Liu, C.H. Wang, G.H. Cao, Microstructures and mechanical properties of Mn modified, ti-nb-based alloys, J. Alloys Compd. 723 (2017) 1091–1097.
[28] M.A. Hussein, C. Suryanarayana, N. Al-Aqeeli, Fabrication of nano-grained ti-nb-zr biomaterials using spark plasma sintering, Mater. Des. 87 (2015) 693–700.
[29] P. Neacsu, D.-M. Gordin, V. Mitran, T. Gloriant, M. Costache, A. Cimpean, In vitro performance assessment of new beta ti-mo-nb alloy compositions, Mater. Sci. Eng. C 47 (2015) 105–113.
[30] A.H. Hussein, M.A.H. Gepreel, M.K. Gouda, A.M. Hefnawy, S.H. Kandil, Biocompatibility of new ti-nb-ta base alloys, Mater. Sci. Eng. C 61 (2016) 574–578.
[31] M. Kikuchi, Y. Takada, S. Kiyosue, M. Yoda, M. Woldu, Z. Cai, O. Okuno, T. Okabe, Mechanical properties and microstructures of cast Ti-Cu alloys, Dent. Mater. 19 (3) (2003) 174–181.
[32] J. Liu, F. Li, C. Liu, H. Wang, B. Ren, K. Yang, E. Zhang, Effect of Cu content on the antibacterial activity of titanium-copper sintered alloys, Mater. Sci. Eng. C 35 (2014) 392–400.
[33] E. Zhang, X. Wang, M. Chen, B. Hou, Effect of the existing form of Cu element on the mechanical properties, bio-corrosion and antibacterial properties of Ti-Cu alloys for biomedical application, Mater. Sci. Eng. C 69 (2016) 1210–1221.
[34] Y. Alshammari, F. Yang, L. Bolzoni, Low-cost powder metallurgy Ti-Cu alloys as a potential antibacterial material, J. Mech. Behav. Biomed. Mater. 95 (2019) 232–239.
[35] J. Liu, X. Zhang, H. Wang, F. Li, M. Li, K. Yang, E. Zhang, The antibacterial properties and biocompatibility of a Ti-Cu sintered alloy for biomedical application, Biomed. Mater. 9 (2) (2014) 025013.
[36] L. Ren, Z. Ma, M. Li, Y. Zhang, W. Liu, Z. Liao, K. Yang, Antibacterial properties of Ti-6Al-4V-xCu alloys, J. Mater. Sci. Technol. 30 (7) (2014) 699–705.

[37] R. Yamanoglu, E. Efendi, F. Kolayli, H. Uzuner, I. Daoud, Production and mechanical properties of Ti-5Al-2.5Fe-xCu alloys for biomedical applications, Biomed. Mater. 13 (2) (2018) 025013.
[38] Y. He, Y. Zhang, Y. Jiang, R. Zhou, Fabrication and characterization of auperelastic Ti-Nb alloy enhanced with antimicrobial Cu via spark plasma sintering for biomedical applications, J. Mater. Res. 32 (13) (2017) 2510–2520.
[39] M. Takahashi, K. Sato, G. Togawa, Y. Takada, Mechanical properties of ti-nb-cu alloys for dental machining applications, J. Funct. Biomater. 13 (4) (2022) 263.
[40] Q. Li, Q. Peng, Q. Huang, M. Niinomi, T. Ishimoto, T. Nakano, Development and characterizations of low-modulus ti-nb-cu alloys with enhanced antibacterial activities, Mater. Today Commun. 38 (2024) 108402.
[41] X. Wang, Z. Li, C. Zhang, H. Hu, J. Ren, Z. Kui, L. Zhang, Z. He, Y. Jiang, Effect of Cu-bearing precipitates on mechanical, wear and antibacterial properties of ti-nb-zr-cu alloy, J. Mater. Res. Technol. 33 (2024) 7938–7948.
[42] C. Torres-Sanchez, F.R.A. Al Mushref, M. Norrito, K. Yendall, Y. Liu, P.P. Conway, The effect of pore size and porosity on mechanical properties and biological response of porous titanium scaffolds, Mater. Sci. Eng. C 77 (2017) 219–228.
[43] Japanese Standards Asociation, Antibacterial Products - Test for Antibacterial Activity and Efficacy, 2010, 2801, 2010.
[44] L. Bolzoni, F. Yang, X-ray diffraction for phase identification in Ti-based alloys: benefits and limitations, Phys. Scri. 99 (6) (2024) 065024.
[45] J.L. Murray, Phase Diagrams of Binary Titanium Alloys, first ed., ASM International1987.
[46] X. He, J.J. Noël, D.W. Shoesmith, Temperature dependence of crevice corrosion initiation on titanium Grade-2, J. Electrochem. Soc. 149 (9) (2002) B440.
[47] Y. Alshammari, N. Elkork, L. Moussa, F. Esmaeil, M. Saeed, M. Alsarraf, A. Alfarhan, M.A. Alrashidi, L. Bolzoni, Systematic review of metal-based alloys with autogenous antibacterial capability, Crit. Rev. Solid State Mater. Sci. 50 (4) (2025) 466–513.
[48] L. Bolzoni, N.H. Babu, Refinement of the grain size of the LM25 alloy (A356) by 96Al-2Nb-2B master alloy, J. Mater. Process. Technol. 222 (2015) 219–223.
[49] A.O.F. Hayama, P.N. Andrade, A. Cremasco, R.J. Contieri, C.R.M. Afonso, R. Caram, Effects of composition and heat treatment on the mechanical behavior of Ti-Cu alloys, Mater. Des. 55 (2014) 1006–1013.
[50] L. Bolzoni, M. Alqattan, F. Yang, L. Peters, Design of β-eutectoid bearing Ti alloys with antibacterial functionality, Mater. Lett. 278 (2020) 128445.
[51] L. Bolzoni, M. Alqattan, L. Peters, Y. Alshammari, F. Yang, Ternary Ti alloys functionalised with antibacterial activity, Sci. Rep. 10 (1) (2020) 22201.
[52] M. Alqattan, L. Peters, Y. Alshammari, F. Yang, L. Bolzoni, Antibacterial ti-mn-cu alloys for biomedical applications, Regen. Biomater. 8 (1) (2020) rbaa050.
[53] M. Alqattan, L. Peters, F. Yang, L. Bolzoni, Microstructure, mechanical behaviour and antibacterial activity of biomedical ti-xmn-ycu alloys, J. Alloys Compd. 856 (2021) 158165.
[54] M. Alqattan, Y. Alshammari, F. Yang, L. Peters, L. Bolzoni, Biomedical ti-cu-mn alloys with antibacterial capability, J. Mater. Res. Technol. 10 (2021) 1020–1028.
[55] R. Boyer, G. Welsch, E.W. Collings, in: A. International (Ed.), Materials Properties Handbook: Titanium Alloys, Ohio, USA, 1998.
[56] S. Raynova, M.A. Imam, F. Yang, L. Bolzoni, Hybrid microwave sintering of blended elemental Ti alloys, J. Manuf. Process. 39 (2019) 52–57.
[57] L. Bolzoni, E.M. Ruiz-Navas, E. Gordo, Investigation of the factors influencing the tensile behaviour of PM Ti-3Al-2.5V alloy, Mater. Sci. Eng. 609 (2014) 266–272.
[58] H.-L. Yang, L. Zou, A.N. Juaim, C.-X. Ma, M.-Z. Zhu, F. Xu, X.-N. Chen, Y.-Z. Wang, X.-W. Zhou, Copper release and ROS in antibacterial activity of Ti-Cu alloys against implant-associated infection, Rare Met. 42 (6) (2023) 2007–2019.
[59] E. Zhang, F. Li, H. Wang, J. Liu, C. Wang, M. Li, K. Yang, A new antibacterial titanium-copper sintered alloy: preparation and antibacterial property, Mater. Sci. Eng., C 33 (2013) 4280–4287.
[60] J.-H. Wu, K.-K. Chen, C.-Y. Chao, Y.-H. Chang, J.-K. Du, Effect of Ti2Cu precipitation on antibacterial property of Ti-5Cu alloy, Mater. Sci. Eng. C 108 (2020) 110433.
[61] C.B. Yi, Z.Y. Ke, L. Zhang, J. Tan, Y.H. Jiang, Z.Y. He, Antibacterial Ti-Cu alloy with enhanced mechanical properties as implant applications, Mater. Res. Express 7 (10) (2020) 105404.